(4 mg) was concentrated by vacuum dialysis against 100 mM KCl, 100 mM NaCl, 5 mM potassium phosphate (pH 6.7) (buffer A) to a final concentration of 1 to 2 mg/ml. TfR was removed and placed on ice, and 20 ml of trypsin (10 mg/ml) was added. After 1 hour, TfR was passed over a benzamidine Sepharose column, and phenylmethysulfonyl fluoride was added (up to 1 mM) to inhibit residual trypsin activity. We then passed the TfR over a Superdex 200 size-exclusion column equilibrated with buffer A to remove aggregated protein.

13. For crystal growth, we concentrated TfR to about 12.5 mg/ml in buffer A. Hanging drops were assembled with 2 ml of TfR and 1 ml of well solution. Wells contained 2.3 to 2.5 M KCl, 10 mM KP_i, and either 1.5 to 2.0% polyethylene glycol (PEG) 6K or 1.2 to 2.0% PEG 20K. Crystals up to 0.5 × 0.4 × 0.3 mm grew over a 3- to 4-week period. Crystals were flash frozen by plunging into liquid N_2 or melting propane. The space group is $P2_12_12_1$, a = 105.4 Å, b = 216.9 Å, c = 361.9 Å. The asymmetric unit contains four TfR dimers, stacked along an 8_5 screw axis coincident with the crystallographic 2_1 parallel to c. Crystals soaked in 1 mM $SmCl_3$ for 24 hours diffracted significantly better than $SmCl_3$-free crystals; $SmCl_3$-soaked crystals were therefore used as native. A real-space heavy-atom search incorporating fourfold noncrystallographic symmetry (NCS) was used to find 16 heavy-atom positions in a di-μ-iodobis(ethylenediamine)diplatinum nitrate derivative (PIP) at 7.0 Å resolution. Single-isomorphous-replacement phases were then used in difference Fourier calculations to find 24 Sm^{3+} positions. Double-isomorphous-replacement phases were calculated by using PIP and $SmCl_3$-free data sets; for the latter, we refined negative Sm^{3+} occupancies. With iterative eightfold averaging and solvent flattening, the phases were refined at 6.0 Å resolution and extended to 3.2 Å. Data were collected on beamline F-1 at the Cornell High-Energy Synchrotron Source (CHESS) either on image plates or on the Quantum-4 CCD detector. All data were processed with the HKL suite (*26*). The data set (from Sm^{3+}-soaked crystals) used for refinement of the model has an overall R_{sym} of 9.9%. The data are essentially complete to 4.0 Å, falling to 32% complete in the outer shell from 3.25 to 3.2 Å, with an R_{sym} for the outer shell of 33.7%. Initial phases were calculated with MLPHARE (*27*), density modification was done with the program DM (*27*), and the model was built with O (*28*). The model has been refined with XPLOR (*22*) using tight NCS restraints (300 Kcal/mol Å^2) with the exception of crystallographic contacts. The apical domain was treated as an NCS group separate from the protease-like and helical domains. The current R_{cryst} and R_{free} for the refined model, using data from 8.0 to 3.2 Å with $I/\sigma(I) >$ 2.0, are 24.0% and 28.7%, respectively. The root-mean-square deviations in bond lengths and bond angles are 0.007 Å and 1.18°. Figs. 1 and 2 were drawn with RIBBONS (*29*), and Fig. 4 was drawn with GRASP (*30*).
14. Letters A to H designate the eight TfR monomers in the crystallographic asymmetric unit. The physiological dimers were identified by the proximity of their NH_2-termini. They are the four pairs AB, CD, EF, and GH related to each other by the 8_5 noncrystallographic symmetry. Each dimer interface has a large solvent-inaccessible surface area of 4100 Å^2. There are also significant contacts between successive dimers within the 8_5 helical columns (2600 Å^2).
15. A. M. Williams and C. A. Enns, *J. Biol. Chem.* **268**, 12780 (1993).
16. B. Chevrier, H. D'Orchymont, C. Schalk, C. Tarnus, D. Moras, *Eur. J. Biochem.* **237**, 393 (1996).
17. A. H. Robbins and C. D. Stout, *Proteins* **5**, 289 (1989).
18. Supplementary material is available at www.sciencemag.org/feature/data/1043272.shl
19. S. Bailey *et al., Biochemistry* **27**, 5804 (1988).
20. B. F. Anderson, H. M. Baker, G. E. Norris, S. V. Rumball, E. N. Baker, *Nature* **344**, 784 (1990); B. J. Anderson, H. M. Baker, G. E. Norris, D. W. Rice, E. N. Baker, *J. Mol. Biol.* **209**, 711 (1989); P. D. Jeffrey *et al., Biochemistry* **37**, 13978 (1998).
21. O. Zak, D. Trinder, P. Aisen, *J. Biol. Chem.* **269**, 7110 (1994); A. B. Mason *et al., Biochem. J.* **326**, 77 (1997).
22. A. T. Brunger, *X-PLOR Version 3.0: A System for Crystallography and NMR* (Yale University Press, New Haven, CT, 1992).
23. S. Kornfield, *Biochemistry* **7**, 945 (1968); D. Hemmaplardh and E. H. Morgan, *Biochim. Biophys. Acta* **426**, 385 (1976); A. B. Mason *et al., Biochemistry* **32**, 5472 (1993).
24. P. K. Bali, O. Zak, P. Aisen, *Biochemistry* **30**, 324 (1991); D. Sipe and R. Murphy, *J. Biol. Chem.* **266**, 8002 (1991).
25. S. Andersson, D. Davis, H. Dahlbäck, H. Jörnvall, D. Russell, *J. Biol. Chem.* **264**, 8222 (1989).
26. Z. Otwinowski and W. Minor, *Methods Enzymol.* **276**, 307 (1997).
27. CCP4, *Acta Crystallogr. D* **50**, 760 (1994).
28. T. A. Jones, J.-Y. Zou, S. W. Cowan, M. W. Kjelgard, *Acta Crystallogr. A* **47**, 110 (1991).
29. M. Carson and C. E. Bugg, *J. Mol. Graph.* **4**, 121 (1986).
30. A. Nichols, K. A. Sharp, B. Honig, *Proteins Struct. Funct. Genet.* **11**, 282 (1991).
31. C. Schneider, M. J. Owen, D. Banville, J. G. Williams, *Nature* **311**, 675 (1984); A. McClelland, L. C. Kuhn, F. H. Ruddle, *Cell* **39**, 267 (1984).
32. F. Buchegger, I. S. Trowbridge, L. S. Liu, S. White, J. F. Collawn, *Eur. J. Biochem.* **235**, 9 (1996).
33. We thank D. Thiel and other staff members at CHESS for assistance with data collection at the F-1 beamline; W. Minor for help in data processing; R. Davis for help with CHO cell expression; P. Aisen, N. Andrews, M. Eck, and M. Wessling-Resnick for discussion; and P. Bjorkman, M. Bennet, and C. Enns for communicating results before publication. C.M.L. is an Armenise Fellow of the Harvard Medical School Center for Structural Biology.

7 July 1999; accepted 8 September 1999

Microtubule Disassembly by ATP-Dependent Oligomerization of the AAA Enzyme Katanin

James J. Hartman and Ronald D. Vale*

Katanin, a member of the AAA adenosine triphosphatase (ATPase) superfamily, uses nucleotide hydrolysis energy to sever and disassemble microtubules. Many AAA enzymes disassemble stable protein-protein complexes, but their mechanisms are not well understood. A fluorescence resonance energy transfer assay demonstrated that the p60 subunit of katanin oligomerized in an adenosine triphosphate (ATP)– and microtubule-dependent manner. Oligomerization increased the affinity of katanin for microtubules and stimulated its ATPase activity. After hydrolysis of ATP, microtubule-bound katanin oligomers disassembled microtubules and then dissociated into free katanin monomers. Coupling a nucleotide-dependent oligomerization cycle to the disassembly of a target protein complex may be a general feature of ATP-hydrolyzing AAA domains.

Microtubules, polymers of α- and β-tubulin subunits, form the mitotic spindle and organize membranous organelles in interphase cells. To accomplish these disparate functions, the microtubule cytoskeleton must rapidly reorganize into different configurations. Microtubules undergo spontaneous growth and shrinkage at their ends, even at steady state, which is important for the cellular rearrangements of these polymers (*1, 2*). In addition to end dynamics, the microtubule wall can be disrupted by the severing enzyme katanin (*3*). Potential in vivo roles for katanin-mediated microtubule severing include releasing microtubules from centrosomes (*4*), depolymerizing microtubule minus ends in the mitotic spindle as a component of poleward flux (*5*), and accelerating microtubule turnover at the G_2/M transition of the cell cycle by creating unstable microtubule ends (*6*).

Katanin is a microtubule-stimulated ATPase, and ATP hydrolysis is required for it to sever and disassemble stable microtubules (*3*). Katanin is a heterodimer organized into a 60-kD enzymatic subunit (p60), which carries out the ATPase and severing reactions, and a targeting subunit (p80), which localizes katanin to the centrosome (*7*). The sequence of p60 reveals that it belongs to the AAA ATPase superfamily, members of which share one or two copies of a conserved 230-amino acid ATPase domain (*8–10*). AAA proteins have been implicated in a myriad of cellular processes as diverse as membrane targeting (NSF, VPS4, p97), organelle biogenesis (PAS1p), proteolysis (SUG1), and transcriptional regulation (TBP1) (*11*). AAA proteins have been proposed to act as nucleotide-dependent chaperones that can disassemble specific protein complexes or unfold polypeptides (*8*). However, little is known about how changes in the nucleotide state of the AAA domain are coupled to the disassembly of their protein targets.

Like the AAA protein NSF (*12, 13*), p60 katanin can form 14- to 16-nm rings, as shown by electron microscopy (*7*). However, p60 (*14*) and GFP-p60, a chimeric protein composed of green fluorescence protein and p60, migrated primarily as 4*S* monomers in 10% to 35% glycerol gradients in the presence of ATP, adenosine diphosphate (ADP), or adenosine-5′-(γ-thio)triphosphate (ATP-γ-S) (Fig. 1A) (*15*).

The Howard Hughes Medical Institute and the Department of Cellular and Molecular Pharmacology, University of California, San Francisco, CA 94143, USA.

*To whom correspondence should be addressed. E-mail: vale@phy.ucsf.edu

GFP-p60 also migrated as a monomer by gel filtration (Stokes radius 66 Å). As a control, an NSF AAA domain (D2) migrated at 8*S* (Fig. 1A), the size expected for a hexamer of 30-kD AAA subunits (*12, 13*). Therefore, in contrast to NSF, p60 does not form stable hexameric rings. Rather, the hydrodynamic and electron microscopy data taken together suggest that p60 monomers and oligomers exist in a reversible equilibrium and that p60 hexameric rings may not be stable to the time and dilution effects of sedimentation and gel filtration.

We examined the dynamics of katanin ring formation in solution as well as in the presence of its microtubule substrate by using a fluorescence resonance energy transfer (FRET)–based assay. To achieve stoichiometric labeling at a defined location on the p60 molecule, we fused p60 to either cyan fluorescent protein (CFP) or yellow fluorescent protein (YFP) as a donor-acceptor pair (*16, 17*). The half-maximal energy transfer distance, R_0, for the CFP and YFP pair is about 5 nm (*18*), which is similar to the intrasubunit distances within the AAA ring (*9, 10*). To test this FRET assay, we prepared an ATP active site mutant (E334Q) (*19*) of CFP-p60 and YFP-p60, which was designed to block nucleotide hydrolysis and trap the enzyme in the ATP-bound state (*20*). An equivalent mutation abolishes the ATPase and membrane fusion activities of NSF (*21*) and promotes oligomerization of VPS4, a single AAA domain protein involved in vacuolar targeting (*22*). As expected, p60^{E334Q} had no detectable ATPase activity. When we mixed CFP-p60^{E334Q} and YFP-p60^{E334Q} fusion proteins in the presence of ADP, no energy transfer occurred and the emission of the CFP-YFP mixture was identical to that when the proteins were tested separately (*14*). However, in solutions that contained ATP, the mixture of CFPp60^{E334Q} and YFP-p60^{E334Q} showed a reduced CFP emission and correspondingly enhanced YFP emission, which is indicative of FRET (Fig. 1B) (*23*). This result indicates that p60^{E334Q} subunits oligomerize when they are complexed with ATP.

To confirm the conclusion from the above FRET experiment, we determined the oligomeric state of CFP-p60^{E334Q} by hydrodynamic analysis. In the presence of ATP, CFP-p60^{E334Q} sedimented at 4*S* and 15*S* in glycerol gradients (Fig. 1A) (*15*). The 15*S* complex dissociated to 4*S* monomers when incubated with 2 mM ADP. To determine the oligomeric state of the 15*S* complex, we performed gel filtration of CFP-p60^{E334Q} in the presence of ATP, which yielded a major peak with a Stokes radius of 8.6 nm (*24*). The Stokes radius and sedimentation coefficient predict a molecular mass of 520 kD, consistent with CFP-p60^{E334Q} forming a hexamer of 90-kD subunits in the presence of ATP. These results agree with the FRET measurements, which also showed ATP-dependent oligomerization of p60^{E334Q}.

We tested microtubules and ATP analogs for their ability to promote oligomerization of wild-type p60. We used the poorly hydrolyzable nucleotide, ATP-γ-S, to mimic the ATP state because it inhibits katanin ATPase activity (*3*) and because both ATP and ATP-γ-S supported similar amounts of FRET in p60^{E334Q} (*14*). Little or no energy transfer occurred in the absence of microtubules regardless of the nucleotide present (Table 1). However, we observed a substantial increase in FRET when we incubated p60 with microtubules and ATP-γ-S but not ADP (Table 1) (*23*). When p60 was not bound to nucleotide (apyrase added), we observed a result similar to that with ADP (*14*). Hence, both nucleotide (ATP) and substrate (microtubules) cooperate in stimulating oligomerization of p60.

To determine the consequences of hexameric ring formation on the interaction of katanin with microtubules, we used a microtubule cosedimentation assay. GFP-p60 bound to microtubules with high affinity ($K_d \sim 0.9$ μM) in the presence of ATP-γ-S, whereas the affinity was reduced to $K_d \sim 18$ μM in the presence of ADP (Fig. 2) (*25*). High-affinity binding may require the microtubule polymer because oligomeric CFP-p60^{E334Q} did not elute with monomeric tubulin on gel filtration columns (*14*). We also assessed the influence of the AAA domain of p60 on microtubule binding. When the AAA domain was deleted, the resultant protein (p60ΔAAA) (*26*) still cosedimented with microtubules, indicating that the NH_2-terminus comprised a microtubule binding domain. Sim-

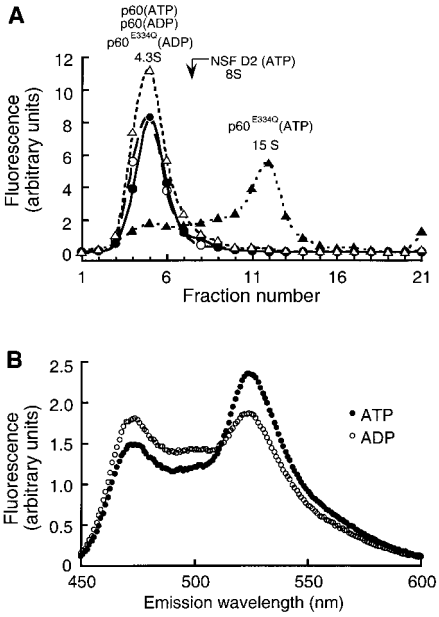

Fig. 1. Oligomerization of p60 katanin. (**A**) Hydrodynamic analysis. Sedimentation profile of GFP-p60 katanin through 10% to 35% glycerol gradients (*15*) in the presence of 2 mM MgATP (closed circles) or MgADP (open circles). Both sediment as a single species of about 4*S*. GFP-p60^{E334Q} (*22*), an active site mutant, was tested in the presence of 2 mM MgATP (closed triangles) and MgADP (open triangles). GFP-p60^{E334Q} sediments as a mixture of 4*S* and 15*S* species in the presence of ATP but as a single species of 4*S* in the presence of ADP. As a control for AAA oligomerization, we sedimented an NSF AAA domain (D2) (*12*) through gradients containing 2 mM MgATP, and the sedimentation peak is indicated by an arrow. (**B**) FRET of a 1:9 mixture of CFP-p60^{E334Q} (donor) and YFP-p60^{E334Q} (acceptor) in the presence of 2 mM MgATP (closed circles) or 2 mM MgADP (open circles) (*22*). FRET is indicated by the decreased emission at 480 nm and the increased emission at 535 nm in the presence of MgATP. The MgADP emission profile is identical to that calculated for CFP-p60^{E334Q} and YFP-p60^{E334Q} measured separately (*14*).

Table 1. Effect of nucleotides and microtubules on CFP-p60–YFP-p60 FRET. MgATP, MgADP, and MgATP-γ-S were present at 2 mM, and microtubules were included at 5 μM where indicated. The FRET signal (*23*) for ADP did not increase at higher (20 μM) microtubule concentrations. FRET values are normalized by using the ADP value as 100% (1.13 for p60^{E334Q}, 0.46 for p60^{wt}). The FRET signals for the p60^{E334Q} and p60^{wt} experiments cannot be directly compared because they were done with slightly different donor/acceptor ratios (p60^{E334Q}, 0.13 μM total; 1:5 ratio of donor CFP to acceptor YFP; p60^{wt}, 0.5 μM total; 1:2 ratio of donor CFP to acceptor YFP). The mean and standard deviation of two measurements (p60^{wt}) or three measurements (p60^{E334Q}) are shown.

Protein	Nucleotide	Microtubules	FRET signal (% of ADP)
p60^{E334Q}	ADP	−	100 ± 1.2
p60^{E334Q}	ATP	−	124 ± 0.9
p60^{wt}	ADP	−	100 ± 0.8
p60^{wt}	ADP	+	102 ± 0.2
p60^{wt}	ATP-γ-S	−	98 ± 0.1
p60^{wt}	ATP-γ-S	+	119 ± 0.2

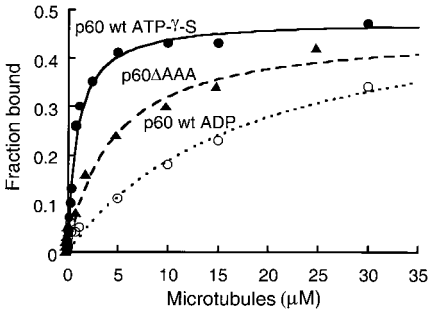

Fig. 2. Nucleotide-dependent binding of p60 katanin to microtubules. Cosedimentation of GFP-p60 and microtubules was tested in the presence of 2 mM MgATP-γ-S (closed circles) ($K_d \sim 0.9$ μM) or MgADP (open circles) ($K_d \sim 18$ μM) (*25*). p60ΔAAA is a truncated p60 that lacks the COOH-terminal AAA domain (closed triangles) ($K_d \sim 6$ μM) (*26*). Binding of this protein was not affected by nucleotide (*14*). Binding is expressed as the fraction of GFP-p60 that cosedimented with microtubules, and the best fit to a hyperbolic curve is shown.

ilarly, protein targeting by NSF also involves its NH_2-terminal domain (*27*). However, p60ΔAAA binding was nucleotide-insensitive (*14*), and its affinity was in between GFP-p60 in its ATP- and ADP-bound states. Thus, the AAA domain of p60 affects the binding affinity of the adjacent microtubule binding domain, and tight binding occurs in nucleotide states (ATP or ATP analogs) that stabilize p60 rings.

Native as well as baculovirus-expressed katanin display an unusual microtubule-stimulated ATPase reaction in which the activity peaks at a microtubule concentration of 2 to 10 μM tubulin dimer and then decreases as the microtubule concentration is further increased (*7*). This differs from the expected Michaelis–Menten hyperbolic stimulation that, for example, is typical of microtubule motor proteins (*28*). One explanation for this behavior is that ATPase activation is driven by hexamer formation and the degree of oligomerization is determined by a competition between p60-p60 and p60 monomer–microtubule associations. To test this possibility, we determined the FRET and ATPase activities of p60 as the microtubule concentration was increased (*29*). Both ATPase activity and FRET increased together as the microtubule concentration was increased and then declined in a similar manner at higher microtubule concentrations (Fig. 3A) (*30*). In agreement with the ATPase measurements, microtubule disassembly by katanin was inhibited at a high microtubule-to-katanin ratio (Fig. 3B) (*31*). These results indicate that microtubules may stimulate the activity of p60 by facilitating p60-p60 interactions. Conversely, high concentrations of microtubules may reduce the ATPase and severing activities by preventing p60-p60 associations through the sequestration of p60 monomers at discontiguous, low-affinity binding sites on the microtubule. The data in Fig. 3 also revealed that release of a tubulin subunit from the microtubule wall requires the hydrolysis of, on average, about 50 ATP molecules. This coupling ratio is similar to that of the chaperone GroEL, which hydrolyzes 50 to 150 ATPs per renaturation of a misfolded protein (*32*).

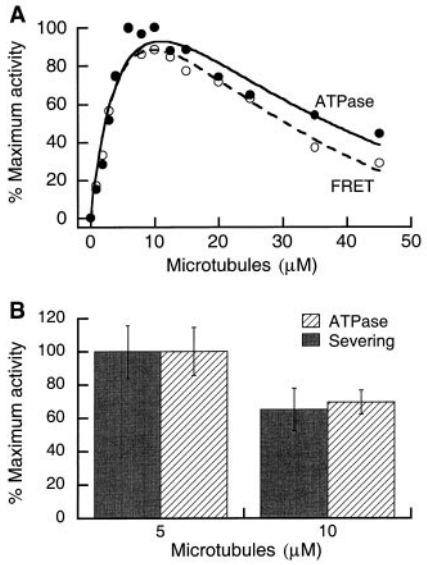

Fig. 3. Effect of microtubules on p60 oligomerization, ATPase, and microtubule severing activities. (**A**) Oligomerization and ATPase activity as a function of microtubule concentration. ATPase activity (closed circles) (*29*) and FRET (open circles) (*23*) were measured in a 0.2 μM, 1:5 mixture of CFP-p60 and YFP-p60. Values have been normalized to the percentage of the maximum observed FRET or ATPase signal. A curve fit is shown for two competing Michaelis–Menten reactions ($\{\{A \times [\text{tubulin}])/(B + [\text{tubulin}]\} - \{(C \times [\text{tubulin}])/(D + [\text{tubulin}])\}\}$). (**B**) Comparison of ATPase (hatched bars) (*29*) and microtubule-disassembly activity (solid bars) (*31*) of 0.2 μM p60 at 5 and 10 μM microtubules. ATPase activity begins to decline above about 2 μM microtubules for untagged p60 (*7*) and above about 10 μM microtubules for CFP-p60–YFP-p60 (Fig. 3A). We used untagged p60 for this assay because microtubule concentrations > 10 μM are not compatible with the fluorescence microtubule disassembly assay. Activities have been normalized to activity at 5 μM, and error bars indicate standard deviation of two measurements. Maximum activity was 1.9 ATP $p60^{-1}$ s^{-1} and 0.04 tubulin dimer $p60^{-1}$ s^{-1}, yielding a coupling ratio of about 50 ATP per tubulin dimer removed from the microtubule.

The above results suggest a model for how katanin disrupts tubulin contacts within a microtubule wall (Fig. 4). Katanin-ADP is monomeric, but nucleotide exchange for ATP enhances p60-p60 affinity. Oligomerization is most efficient, however, in the presence of its protein substrate, which suggests that microtubules act as a scaffold for promoting oligomerization. The p60 ring then binds to microtubules with high affinity, potentially as a result of forming multiple tubulin contacts. Once katanin oligomers assemble on the microtubule, ATPase activity is stimulated. Nucleotide hydrolysis and subsequent phosphate release could change the conformation of the katanin ring, leading to mechanical strain that destabilizes tubulin-tubulin contacts (Fig. 4). Consistent with this idea, large conformational changes have been observed for the NSF ring in its ATP and ADP states (*12*). A concerted conformational change also occurs for the chaperone GroEL, which binds misfolded polypeptides at multiple sites within its seven-membered ring and undergoes large interdomain motions that strain the bound polypeptide (*33, 34*). Alternatively, as described for the microtubule-destabilizing kinesin XKCM1 (*35*), tight binding of katanin oligomers could strain tubulin-tubulin contacts, with ATP hydrolysis serving to dissociate katanin-tubulin dimers from this stable complex. In either scenario, ATP hydrolysis also serves a recycling function because p60-p60 and p60-tubulin interactions both weaken in the ADP-bound state, dissociating tubulin and releasing p60-ADP to begin a new round of disassembly. This proposed cycle has similarities to that of dynamin, which self-assembles into a spiral pattern on endocytic membrane tubules, changes conformation after hydrolysis of guanosine triphosphate in a manner that vesiculates the tubule, and then disassembles in the guanosine diphosphate state (*36*).

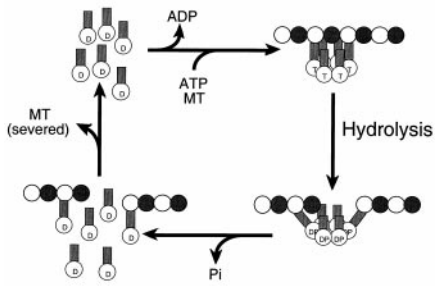

Fig. 4. Model for microtubule severing by katanin. See text for detail of the mechanism. For simplicity, only a single protofilament of the microtubule is shown. T, DP, and D represent ATP, ADP + P_i, and ADP states, respectively. The relatively low affinity of katanin for nucleotide suggests that exchange of ATP for ADP would occur rapidly in solution. The conformational change is shown to occur with γ-phosphate bond cleavage, although this could also occur as a result of γ-phosphate release.

The oligomerization cycle described for katanin also may occur in many other AAA enzymes. ATP enhances oligomerization of VPS4, a single AAA domain protein, and it was proposed that this oligomerization could be further facilitated by an as yet unidentified membrane-associated target (*22*). Such reactions could be tested by the FRET-based assay described here. In contrast to katanin and VPS4, NSF is a constitutive hexamer (*13*) because of the presence of an additional nonhydrolytic AAA domain (D2) (*21*). Our results, however, raise the possibility that the ATP-hydrolyzing AAA domains (D1) may undergo cycles of tight and weak interactions while remaining tethered through their D2 domains. Thus, nonhydrolyzing AAA domains may serve as anchors to keep the enzymatic subunits in close proximity throughout the hydrolytic cycle.

References and Notes

1. T. Mitchison and M. Kirschner, *Nature* **312**, 237 (1984).
2. A. B. Desai and T. J. Mitchison, *Annu. Rev. Cell Dev. Biol.* **13**, 83 (1997).
3. F. J. McNally and R. D. Vale, *Cell* **75**, 419 (1993).
4. T. J. Keating *et al., Proc. Natl. Acad. Sci. U.S.A.* **94**, 5078 (1997); F. J. Ahmad, W. Yu, F. J. McNally, P. W. Bass, *J. Cell Biol.* **145**, 305 (1999).
5. T. J. Mitchison, *J. Cell Biol.* **109**, 637 (1989).
6. Y. Zhai, P. J. Kronebusch, P. M. Simon, G. G. Borisy, *ibid.* **135**, 201 (1996).
7. J. J. Hartman *et al., Cell* **93**, 277 (1998).
8. F. Confalonieri and M. Duguet, *Bioessays* **17**, 639 (1995); A. Morgan and R. D. Burgoyne, *Trends Cell Biol.* **5**, 335 (1995); K. Leonhard, A. Stiegler, W. Neupert, T. Langer, *Nature* **398**, 348 (1999).
9. C. U. Lenzen, D. Steinmann, S. W. Whiteheart, W. I. Weis, *Cell* **94**, 525 (1998).
10. R. C. Yu, P. I. Hanson, R. Jahn, A. T. Brunger, *Nature Struct. Biol.* **5**, 803 (1998).

11. S. Patel and M. Latterich, *Trends Cell Biol.* **8**, 65 (1998).
12. P. I. Hanson *et al.*, *Cell* **90**, 523 (1997).
13. K. G. Fleming *et al.*, *J. Biol. Chem.* **273**, 15,675 (1998).
14. J. J. Hartman and R. D. Vale, data not shown.
15. Katanin p60 was cloned into the Bam HI site of pFastBac HT B (Life Technologies). The resulting baculovirus construct expresses p60 (amino acids 1 to 516) with the following additional NH_2-terminal amino acids: MSYYHHHHHHDYDIPTTENLYFQGS. The GFP mut2 [B. P. Cormack *et al.*, *Gene* **173**, 33 (1996)] coding sequences were amplified with primers containing Kas I sites at both ends and inserted into the Kas I site in pFastBac HT B. The resulting baculovirus constructs express GFP fused to the NH_2-terminus of p60. We prepared recombinant p60 proteins as described in (*7*), except that we did not perform Mono Q chromatography, and the proteins were stored at −80°C in Ni-NTA elution buffer [20 mM tris (pH 8.0), 100 mM NaCl, 100 mM imidazole, 2 mM $MgCl_2$, 0.02% Triton X-100, 10 mM 2-mercaptoethanol, 10% glycerol, 250 μM ATP]. Storage in ATP was necessary to preserve enzyme activity. Glycerol gradient centrifugation was modified from other methods (*12*). Gradients were prepared by layering equal steps of 10%, 16.3%, 22.5%, 28.8%, and 35% glycerol in gradient buffer [20 mM potassium Hepes (pH 8.0), 75 mM potassium glutamate, 2 mM $MgCl_2$, 0.02% Triton X-100, 1 mM dithiothreitol], with the indicated nucleotide (2 mM) and equimolar $MgCl_2$; gradients were allowed to form overnight at 4°C. Proteins in Ni-NTA elution buffer were diluted ~1:1 with gradient buffer (final concentration, ~5 μM) and incubated with the appropriate nucleotide (2 mM) and 2 mM $MgCl_2$ for 15 min on ice before centrifugation. The NSF D2 domain was expressed and purified as described in (*12*) and handled as described above. Bovine serum albumin (BSA) (4.1*S*), catalase (11.2*S*), and thyroglobulin (19.4*S*) were used as standards. Gradients were centrifuged for 12 hours at 285,000*g* in an SW60 Ti rotor (Beckman Instruments) at 4°C. GFP-tagged p60 was quantitated by fluorescence (λ_{ex} 470, λ_{em} 508) using either an SLM 8100 in photon counting mode (Spectronics) or a Perkin-Elmer LS-5B (Perkin-Elmer). Standards and NSF D2 were quantitated by the Bradford assay.
16. A. Miyawaki *et al.*, *Nature* **388**, 882 (1997).
17. ECFP (Clonetech) and EYFP (Clonetech) coding sequences were inserted into the pFastBac-p60 expression plasmid as in (*15*).
18. R. Tsien, personal communication.
19. Amino acid residues are abbreviated as follows: A, Ala; C, Cys; D, Asp; E, Glu; F, Phe; G, Gly; H, His; I, Ile; K, Lys; L, Leu; M, Met; N, Asn; P, Pro; Q, Gln; R, Arg; S, Ser; T, Thr; V, Val; W, Trp; Y, Tyr.
20. The E334Q mutant was prepared by overlap extension amplification [S. N. Ho *et al.*, *Gene* **77**, 51 (1989)] of the wild-type p60 cDNA, followed by cloning of the mutant sequence into pFastBac HT B as in (*15*) and sequencing to check for amplification errors.
21. S. W. Whiteheart *et al.*, *J. Cell Biol.* **126**, 945 (1994).
22. M. Babst, B. Wendland, E. J. Estepa, S. D. Emr, *EMBO J.* **17**, 2982 (1998).
23. Separately purified CFP-p60 and YFP-p60 were preincubated together in the indicated ratios at a 10× assay concentration for 30 to 60 min on ice. The CFP-YFP–p60 mixture was then diluted into reaction mixtures containing 2 mM nucleotide and equimolar $MgCl_2$ in ATPase buffer [20 mM potassium Hepes (pH 7.5), 25 mM potassium glutamate, 2 mM $MgCl_2$, 0.02% Triton X-100, 10% glycerol, 20 μM paclitaxel]. Reaction mixtures contained BSA at 1 mg/ml to prevent surface adsorption; 20 mM glucose and hexokinase at 0.1 mg/ml, which converted residual ATP to ADP, were used to measure FRET in the ADP state. For FRET measurements with microtubules, we preincubated p60 with the nucleotide mixture for 10 min at 22°C before we added microtubules. Microtubules were prepared in ATPase buffer containing 20 μM paclitaxel, as described in (*7*). After a 10- to 15-min incubation with microtubules, we quantitated energy transfer by exciting the sample at 433 nm and measuring the fluorescence at 480 and 535 nm. We used the ratio of emission at 535 nm/480 nm as the measure of energy transfer (*16*). For emission scans, we excited the sample at 433 nm and measured the fluorescence emission between 450 and 600 nm with excitation and emission slit sizes of 1 nm.
24. We performed gel filtration chromatography on about 15 μg of $p60^{E334Q}$ with a 0.78 × 30 cm TSK-4000SWXL column (TosoHaas) equilibrated with 20 mM potassium Hepes (pH 7.8), 75 mM potassium glutamate, 2 mM $MgCl_2$, 0.02% Triton X-100, 5% glycerol, and 1 mM ATP. Standard proteins were BSA (Stokes radius 35 Å), catalase (52 Å), and thyroglobulin (86 Å). We estimated molecular mass by using the measured Stokes radius and the *S* value [L. M. Siegel and K. J. Monty, *Biochim. Biophys. Acta* **112**, 346 (1966)].
25. GFP-p60 (0.4 μM final concentration) was mixed with paclitaxel-stabilized microtubules prepared as in (*7*) and BSA (1 mg/ml) in ATPase buffer and incubated at 22°C for 20 min. We used 5 mM glucose and hexokinase (0.1 mg/ml), which converted residual ATP to ADP, to measure binding in ADP. Samples (50 μl) were incubated at 22°C for 20 min before loading onto a 50-μl cushion of 66% glycerol in ATPase buffer, followed by centrifugation for 5 min at 436,000*g* (20°C). The supernatant and cushion were removed and diluted 1:1 with water to reduce sample viscosity. The microtubule pellets were depolymerized by incubation on ice for 30 min in ATPase buffer containing 5 mM $CaCl_2$, followed by 1:1 dilution with water. Bound and free GFP-p60 were determined by fluorescence (λ_{ex} 470, λ_{em} 508).
26. The p60ΔAAA construct was prepared by amplifying the region coding for amino acids 1 to 210 of p60 and inserting this into pFastBac HT B at the Bam HI and Xho I sites. We amplified the GFP coding sequence and inserted it at Kpn I and Hind III sites, which resulted in a baculovirus that expresses p60 (amino acids 1 to 210) with the same additional NH_2-terminal amino acids as wild-type p60 fused to the NH_2-terminus of GFP.
27. E. E. Nagiec, A. Bernstein, S. W. Whiteheart, *J. Biol. Chem.* **270**, 29182 (1995).
28. S. P. Gilbert and K. A. Johnson, *Biochemistry* **32**, 4677 (1993).
29. We performed ATPase assays by using the malachite green method as described in (*7*). We included DEAE-purified ATP at 1 mM.
30. We also examined FRET when the katanin concentration was varied with a constant microtubule concentration in the presence of ATP-γ-S. The signal did not increase in a hyperbolic manner. Instead, an increase in the FRET signal was observed only when the katanin reached a critical concentration, which again suggests a cooperative phenomenon.
31. We measured the microtubule severing rate with a fluorescence-based assay for 4′,6-diamidino-2-phenylindole binding as described in (*7*). To calculate the amount of tubulin dimers released, we divided the rate of change of fluorescence ($\Delta F/s$) by {[($F_{unsevered}$) − ($F_{Ca^{2+}\ depolymerized}$)]/microtubule concentration, μM}.
32. P. B. Sigler *et al.*, *Annu. Rev. Biochem* **67**, 581 (1998).
33. Z. Xu, A. L. Horwich, P. B. Sigler, *Nature* **388**, 741 (1997).
34. M. Shtilerman, G. H. Lorimer, S. W. Englander, *Science* **284**, 822 (1999).
35. A. Desai, S. Verma, T. J. Mitchison, C. E. Walczak, *Cell* **96**, 69 (1999).
36. S. M. Sweitzer and J. E. Hinshaw, *ibid.* **93**, 1021 (1998).

37. We thank F. J. McNally, R. D. Mullins, K. S. Thorn, and J. E. Wilhelm for critical reading of the manuscript.

29 July 1999; accepted 14 September 1999

Neuronal Activity-Dependent Cell Survival Mediated by Transcription Factor MEF2

Zixu Mao,[1]* Azad Bonni,[1] Fen Xia,[2] Mireya Nadal-Vicens,[1] Michael E. Greenberg[1]†

During mammalian development, electrical activity promotes the calcium-dependent survival of neurons that have made appropriate synaptic connections. However, the mechanisms by which calcium mediates neuronal survival during development are not well characterized. A transcription-dependent mechanism was identified by which calcium influx into neurons promoted cell survival. The transcription factor MEF2 was selectively expressed in newly generated postmitotic neurons and was required for the survival of these neurons. Calcium influx into cerebellar granule neurons led to activation of p38 mitogen-activated protein kinase-dependent phosphorylation and activation of MEF2. Once activated, MEF2 regulated neuronal survival by stimulating MEF2-dependent gene transcription. These findings demonstrate that MEF2 is a calcium-regulated transcription factor and define a function for MEF2 during nervous system development that is distinct from previously well-characterized functions of MEF2 during muscle differentiation.

The MEF2 proteins constitute a family of transcription factors that play a critical role in the process of cell differentiation during the development of multicellular organisms (*1–7*). MEF2 proteins cooperate with members of the MyoD family in specifying the differentiation of skeletal muscle (*8, 9*). During neurogenesis, MEF2 mRNAs are robustly transcribed in the developing mammalian central nervous system (CNS) (*10–12*), although the functions of MEF2s during nervous system development have not been known.

To investigate the role of the MEF2 proteins during mammalian CNS development, we first characterized the expression of

[1]Division of Neuroscience, Department of Neurology, Children's Hospital and Department of Neurobiology, Harvard Medical School, Boston, MA 02115, USA. [2]Department of Radiation Oncology, Massachusetts General Hospital, Charlestown, MA 02129, USA.

*Current address: The Liver Research Center, Rhode Island Hospital and Department of Medicine, Brown University Medical School, Providence, RI 02903, USA. †To whom correspondence should be addressed. E-mail: greenberg@a1.tch.harvard.edu